Food Chemistry 211 (2016) 819–826

Contents lists available at ScienceDirect

Food Chemistry

journal homepage: www.elsevier.com/locate/foodchem

Complexes between ovalbumin nanoparticles and linoleic acid: Stoichiometric, kinetic and thermodynamic aspects

Osvaldo E. Sponton [a,b], Adrián A. Perez [a,b], Carlos R. Carrara [b], Liliana G. Santiago [b,*]

[a] Consejo Nacional de Investigaciones Científicas y Técnicas de la República Argentina (CONICET), Argentina
[b] Área de Biocoloides y Nanotecnología, Instituto de Tecnología de Alimentos, Facultad de Ingeniería Química, Universidad Nacional del Litoral, 1 de Mayo 3250 (3000), Santa Fe, Argentina

ARTICLE INFO

Article history:
Received 4 April 2016
Received in revised form 19 May 2016
Accepted 21 May 2016
Available online 24 May 2016

Keywords:
Linoleic acid
Ovalbumin nanoparticles
Physical adsorption
Stoichiometry
Kinetics
Thermodynamics
Atomic Force Microscopy

ABSTRACT

Stoichiometric, kinetic and thermodynamic aspects of complex formation between heat-induced aggregates of ovalbumin (ovalbumin nanoparticles, OVAn) and linoleic acid (LA) were evaluated. Extrinsic fluorescence data were fitted to modified Scatchard model yielding the following results: n: 49 ± 2 LA molecules bound per OVA monomer unit and K_a: 9.80 ± 2.53 × 10^5 M. Kinetic and thermodynamic properties were analyzed by turbidity measurements at different LA/OVA monomer molar ratios (21.5–172) and temperatures (20–40 °C). An adsorption approach was used and a pseudo-second-order kinetics was found for LA-OVAn complex formation. This adsorption process took place within 1 h. Thermodynamic parameters indicated that LA adsorption on OVAn was a spontaneous, endothermic and entropically-driven process, highlighting the hydrophobic nature of the LA and OVAn interaction. Finally, Atomic Force Microscopy imaging revealed that both OVAn and LA-OVAn complexes have a roughly rounded form with size lower than 100 nm.

1. Introduction

In the last years, development of nutraceutical vehiculization systems has gained considerable interest in food industry (Perez, Sponton, Andermatten, Rubiolo, & Santiago, 2015; Zimet & Livney, 2009). In this sense, several strategies to incorporate these compounds in food aqueous matrices have been evaluated (Gutiérrez et al., 2013; McClements & Li, 2010). One of them includes the formation of ligand-protein complexes, being the ligand a nutraceutical compound. Moreover, biopolymer nanoparticles can be produced by polysaccharide electrostatic deposition onto the surface of preformed ligand-protein complexes in order to improve colloidal stability and nutraceutical protection against environmental conditions such as oxygen, UV radiation, etc. (Perez et al., 2015; Zimet & Livney, 2009).

Overall, ligand-protein interactions are characterized by means of the binding parameters, n and K_a, which represent the binding stoichiometry and association constant, respectively (Joye, Davidov-Pardo, Ludescher, & McClements, 2015; Le Maux, Bouhallab, Giblin, Brodkorb, & Croguennec, 2013; Wang et al., 2013). In some cases, thermodynamic parameters such as enthalpy, entropy and free energy changes associated to ligand-protein complexes formation are also informed (Moyon, Islam, Phukan, & Mitra, 2013; Wang et al., 2013). Ligand-protein interactions can be analyzed by using several techniques such as intrinsic (Sponton, Perez, Carrara, & Santiago, 2015a) and extrinsic fluorescence spectroscopy (Lange, Kothari, Patel, & Patel, 1998), equilibrium dialysis (Muresan, van der Bent, & de Wolf, 2001), and currently, by isothermal titration calorimetry (Le Maux et al., 2013). However, at the present, fluorescence technique is the most widely used method.

In literature, there are a lot of works which characterize ligand-protein interactions in order to determine the intrinsic ability of native proteins to bind hydrophobic and hydrophilic ligands (Joye et al., 2015; Rhodes et al., 2014; Wang et al., 2013). About this, β-lactoglobulin (BLG) is one of the most studied proteins (Le Maux et al., 2013; Perez, Andermatten, Rubiolo, & Santiago, 2014; Perez et al., 2015; Sponton, Perez, Carrara, & Santiago, 2014; Zimet & Livney, 2009). However, studies of interaction between ligands and heat-induced protein aggregates have gained relevance. Moreover, it is well known that protein denaturation/aggregation processes lead to an increase in surface hydrophobicity under certain heat treatment conditions. Thus, higher surface hydrophobicity of protein aggregates can promote greater ligand binding capacity than native proteins (Croguennec, Renault, Beaufils, Dubois, & Pezennec, 2007; Le Maux et al., 2013; Perez

* Corresponding author.
E-mail address: lsanti@fiq.unl.edu.ar (L.G. Santiago).

http://dx.doi.org/10.1016/j.foodchem.2016.05.137
0308-8146/

et al., 2014; Sponton, Perez, Carrara, & Santiago, 2015b; Sponton et al., 2015a).

In a previous work, it was demonstrated that controlled heat treatment of ovalbumin (OVA) dispersion produced ovalbumin aggregates with a mean hydrodynamic diameter lower than 100 nm (ovalbumin nanoparticles, OVAn). These nanoparticles presented higher surface hydrophobicity and higher LA binding ability than native OVA. Moreover, from fluorescence and ζ-potential analysis, it was found that LA binds to OVAn by means of hydrophobic interaction (Sponton et al., 2015a); however, quantitative parameters were not determined. Hence, in order to quantify parameters associated to LA-OVAn interaction, additional studies should be performed taking into account stoichiometric, kinetic and thermodynamic aspects. The knowledge of these parameters would allow reaching a better understanding of the LA-OVAn complexes formation.

Linoleic acid is a polyunsaturated fatty acid (PUFA) which is essential to human diet because is not synthesized endogenously by humans. PUFAs play an important role in cardiovascular and inflammatory disease, mental health and brain development and function (Ruxton, Reed, Simpson, & Millington, 2004). In general, fatty acids have very low water solubility, which limit their incorporation in aqueous systems. On the other hand, they can form supramolecular structures (micelles, vesicles, etc.) in some buffer solutions, resulting in stable colloidal dispersion with appreciable turbidity (Fontana, Spolaore, & Polverino de Laureto, 2013; Sponton et al., 2015a). Moreover, PUFAs are susceptible to oxidative deterioration (Fioramonti, Arzeni, Pilosof, Rubiolo, & Santiago, 2015), so that complexation with protein could be a strategy for protect them.

In this context, the aim of the present work was to evaluate the stoichiometric, kinetic and thermodynamic aspects of LA-OVAn complex formation. This information would allow defining the most appropriate conditions to produce innovative nutraceutical vehiculization systems. For this, a set of complementary techniques and models were employed, including an adsorption mechanism to describe LA-OVAn complexes formation. Finally, AFM images were also included in order to describe some morphological and structural aspects.

2. Materials and methods

2.1. Materials

Ovalbumin (product A5503, purity 98% according to agarose gel electrophoresis) and linoleic acid (LA) samples were obtained from Sigma (USA). Extrinsic fluorescence probe, 1-anilino-8-naphthalene sulfonic acid (ANS), was purchased from Fluka Chemie AG (Switzerland).

2.2. Ovalbumin nanoparticles obtention

Ovalbumin nanoparticles (OVAn) were obtained by heat treatment (85 °C, 5 min) of 10 g/L OVA solution at pH 7.5 and 50 mM NaCl according to a previous work (Sponton et al., 2015a). The obtained OVA nanoparticles showed a monomodal particle size distribution (determinated by dynamic light scattering, DLS) with peak: 79 nm and polydispersity index (PdI): 0.208 as described in Sponton et al. (2015a).

2.3. Binding stoichiometry

In order to study LA-OVAn binding stoichiometry, fluorescence and turbidity (absorption at 400 nm) measurements were done. It is important to remark that binding parameters were expressed on the basis of OVA monomeric unit (i.e. considering individual OVA macromolecules), due to the ovalbumin aggregates are formed by the association of OVA molecules (Le Maux et al., 2013).

2.3.1. Fluorescence measurements

In order to determine the binding stoichiometry, i.e. number of LA molecules bound per OVA monomeric unit (n) and the association constant (K_a), an extrinsic fluorescence method was applied. For this, samples were prepared adding increasing volumes of 15 mM LA ethanolic solution to 2 ml of 0.043 g/L OVAn solution in 50 mM pH 7 potassium phosphate buffer. Then, 9 μL of 15 mM ANS solution was added to each sample. This experiment was performed under the assumption that ANS would not displace LA molecules from the LA-OVAn complexes (Lange et al., 1998; Takikawa & Kaplowitz, 1986). Emission spectra were registered between 410 and 600 nm, at 390 nm excitation wavelength by using a Hitachi F-2000 fluorescence spectrophotometer (Japan) (Croguennec et al., 2007; Sponton et al., 2015a). Experiments were performed in triplicate at room temperature (around 20 °C). ANS maximum emission fluorescence intensity (F) for each spectrum was registered, and relative fluorescence (RFI-ANS) was calculated as the ratio between F at a given LA concentration, and F at zero LA concentration (F_0). Titration curves were plotted as RFI-ANS *versus* LA concentration, and data were fitted to the modified Scatchard model:

$$[P] \cdot (1 - f_i) = \frac{[L]}{n} \cdot \left(\frac{1}{f_i}\right) - \frac{1}{K_a \cdot n} \quad (1)$$

where [P] is the total molar protein concentration (based on OVA monomer); [L] is the total molar ligand concentration; n is the number of ligand molecules bound to protein at the saturation and f_i is defined as:

$$f_i = \frac{F - F_0}{F_{max} - F_0} \quad (2)$$

where F_{max} is the fluorescence intensity at saturation. It is important to highlight that when F_{max} is not reached experimentally, its value can be determined by data fitting to an exponential decay model (Le Maux et al., 2013).

2.3.2. Turbidity measurements

In previous works, it was reported that LA dispersed in phosphate buffer showed appreciable turbidity as a consequence of supramolecular self-assemblies formation. However, when OVAn is added to LA dispersion, turbidity decreased as a consequence of the disassembly of micelles in favor of interaction with protein (LA-OVAn complexes formation) forming a stable colloidal system (Sponton et al., 2015a, 2015b). In the present paper, we have extended such studies for deepening the knowledge about binding stoichiometry of the LA-OVAn complex formation. Thus, turbidity of LA dispersions was determined as the absorbance (ABS) at 400 nm using a Jenway 7305 Spectrophotometer (UK). Systems were prepared adding increasing volumes of 100 mM LA ethanolic solution to 2 ml of 0.5 g/L OVAn in 50 mM pH 7 potassium phosphate buffer solution, up to 1.2 mM maximum total LA concentration. Measurements were performed at room temperature (~20 °C) in triplicate.

2.4. Kinetics of complex formation

Kinetics of LA-OVAn complexes formation was analyzed by means of a turbidity approach. Turbidity measurements were carried out in a Perkin Elmer Lambda 20 UV/Vis Spectrometer (USA) equipped with a water thermo-circulator. Determinations were performed in a temperature range of 20–40 °C. In first place,

2.4 mL of LA solution (1.25 mM in 50 mM pH 7 potassium phosphate buffer) were placed in the measuring cell, and turbidity (ABS at 400 nm) was registered as a function of time. After ~30 s, 0.6 mL of OVAn solution was added into the measuring cell and the system was mixed in order to reach homogeneity. Different LA/OVA monomer molar ratios (L/P, 21.5–172) were prepared. As it was mentioned previously, when OVAn is added to LA dispersion its turbidity decreases (Sponton et al., 2015a). Time at which turbidity started to decrease was taken as zero. Results were reported as relative turbidity, which was defined as the ratio between turbidity at a given time and the turbidity at zero time. Measurements were performed at least in duplicate.

Turbidity time evolution was analyzed taken into account a batch adsorption process without agitation, in which OVAn and LA were taken as adsorbent and adsorbate, respectively. For the data analysis, the following mass balance was proposed (Yao & Chen, 2015):

$$L - L_t = q_t \cdot m \tag{3}$$

where L is the total amount of LA mol (obtained from turbidity at zero time); L_t is non-adsorbed amount of LA mol in the bulk at time t (obtained from turbidity at a given time); q_t is the adsorbed amount of LA mol by mass unit of adsorbent at a given time; m is the adsorbent mol (OVA monomer). At time in which adsorption equilibrium is reached, q_t is defined as q_e, i.e. adsorbed amount of LA mol by mass unit of OVAn at equilibrium (Yao & Chen, 2015).

Experimental data (Turbidity *versus* time) were fitted to two adsorption kinetic models: pseudo-first-order and pseudo-second-order kinetic models (Eqs. (4) and (5), respectively) (Yao & Chen, 2015):

$$-\ln\left(1 - \frac{q_t}{q_e}\right) = k_1 \cdot t \tag{4}$$

$$q_t = \frac{k_2 \cdot q_e^2 \cdot t}{1 + k_2 \cdot q_e \cdot t} \tag{5}$$

where k_1 and k_2 are the pseudo-first-order and the pseudo-second-order rate constant, respectively, and t is the time. The k_1 value is obtained by means of simple linear regression of $[-\ln(1 - q_t/q_e)]$ *versus* t; whereas the kinetic parameters for the pseudo-second-order kinetic model can be obtained from its linear form:

$$\frac{t}{q_t} = \frac{1}{k_2 \cdot q_e^2} + \frac{t}{q_e} \tag{6}$$

In Eq. (6) can be observed that $1/q_e$ is the slope and $1/k_2 \cdot q_e^2$ is the intercept.

2.5. Atomic Force Microscopy

For atomic force microscopy (AFM) measurements, aliquots of 2 μl of sample (dilution: 0.01 g/L), were adsorbed to a cleaved mica surface (1 cm^2) (glued to steel disks) by means of a dry step in vacuum chamber at room temperature and protected against light to avoid LA deterioration. AFM imaging was performed in air in tapping mode by an Agilent 5400 microscope (USA). Backside silicon and aluminum coated AFM cantilevers (Budget Sensors; model: Tap300Al-G, Bulgaria) with the following specifications were used: length: 125 μm; tip radius: <10 nm; mean width: 30 ± 5 μm; thickness: 4 ± 1 μm; tip height: 17 ± 2 μm; tip set back: 15 ± 5 μm; spring force constant: 40 N/m. A cantilever oscillation frequency of 280 kHz was employed. Samples were scanned at 1 line/s. For processing images, Gwyddion 2.44 software was used. AFM topography images are showed and besides, the corresponding phase images are presented in order to show a better definition of particles.

2.6. Statistical analysis

Statistical differences were determined by means of one way analysis of variance (ANOVA) using the StatGraphics Centurion XV software. LSD test at 95% confidence level was applied.

3. Results and discussion

3.1. Stoichiometry of LA-OVAn complexes formation

3.1.1. Extrinsic fluorescence measurements

ANS fluorescence spectra of OVAn dispersion for different LA concentration are shown in Fig. 1A. ANS fluorescence intensity decreased with the increase in LA concentration. This behavior can be explained taking into account that ANS fluorescence occurs due to the non-covalent union of the probe to hydrophobic sites on protein (Albani, 2004; Perez, Carrera Sánchez, Rodríguez Patino, Rubiolo, & Santiago, 2012). Moreover, LA also binds to hydrophobic sites on OVAn. Hence, when LA-OVAn complexes are formed, lower amount of hydrophobic sites on OVAn would be available for binding ANS molecules, and consequently, ANS fluorescence decrease (Sponton et al., 2015a). Fig. 1B displays the RFI-ANS of OVAn dispersions as a function of LA concentration. In this Figure, intrinsic fluorescence data were also included (RFI values obtention is described in Sponton et al., 2015a). It has hypothesized that the RFI-ANS *versus* LA concentration curve would represent the fraction of total hydrophobic sites which were not filled by LA and consequently, they were filled by ANS; whereas the RFI *versus* LA concentration curve would represent the fraction of intrinsic fluorophore hydrophobic sites which were not filled by LA. It is important to remark that intrinsic fluorophore hydrophobic sites would be only a fraction of total hydrophobic sites on the protein nanoparticles. As it can be noted in Fig. 1B, both RFI-ANS and RFI reached a constant value at ~75 μM LA concentration (saturation conditions). However, the decrease in RFI-ANS with the increase in LA concentration was greater than RFI. It was noted that RFI decreased ~30% while RFI-ANS decreased ~70%. These results would indicate that LA molecules would bind not only to hydrophobic sites with intrinsic fluorophores but also to other hydrophobic sites.

On the other hand, the lowest RFI-ANS value at saturation (~0.3) would indicate that there were still some hydrophobic sites which were not filled by LA. This could mean that LA-OVAn binding would require the presence of hydrophobic pockets with a particular spatial disposition of the amino acid residues on the protein nanoparticle surface (Le Maux et al., 2013; Perez et al., 2014; Sponton et al., 2014). Hydrophobic sites which did not meet this characteristic were filled by ANS and they were responsible for the extrinsic fluorescence at saturation of OVAn. Taking into account that the decrease in extrinsic fluorescence is due to the increase in LA concentration (Fig. 1B), the modified Scatchard model (Eq. (1)) was applied for obtaining binding parameters. It was observed a good fitting (R^2 = 0.987 ± 0.011) yielding the following binding parameters: n: 49 ± 2 and K_a: 9.80 ± 2.53 × 10^5 M. Moreover, there was significant red shift behavior at the ANS maximum emission wavelength (data not shown), which could suggest that ANS was bound in an increasingly polar environment. These results would suggest that the binding mode of LA to OVAn could respond to an inside-out saturation mechanism in which inner sites (non-polar or hydrophobic) are firstly filled.

On the other hand, taking into account that ANS is a fluorophore which binds to all protein hydrophobic sites, the studies of ligand binding to proteins using fluorescence would not be limited to the presence of an intrinsic fluorophore at the ligand binding site.

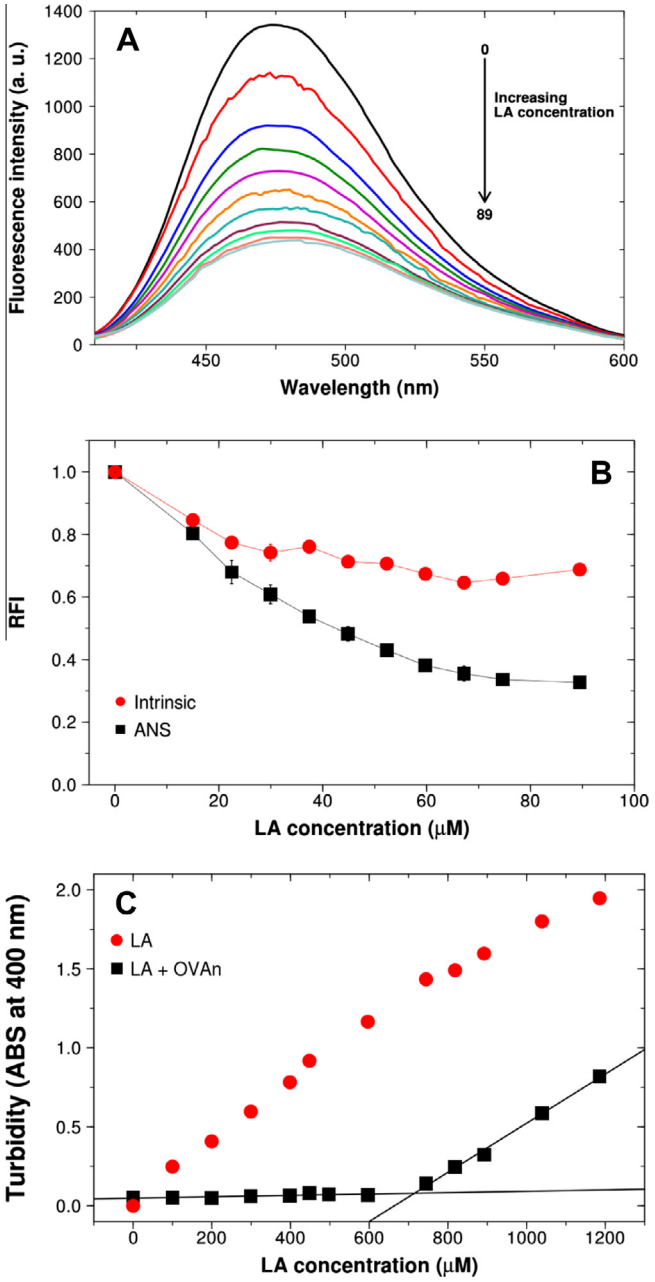

Fig. 1. A: Extrinsic (ANS) fluorescence spectra of OVAn-LA systems (ex: 390 nm). B: Relative extrinsic (ANS) fluorescence and intrinsic intensity of OVAn-LA systems. OVAn concentration: 0.043 g/L (1 μM as monomer OVA units) (b). Measurements were carried out at room temperature (~20 °C). Relative intrinsic fluorescence intensity of OVAn-LA systems at different temperatures. Ex: 280 nm. OVAn concentration: 0.043 g/L (1 μM as OVA monomer units). C: Turbidity (ABS at 400 nm) of LA dispersions with and without 0.5 g/L OVAn (11.6 μM as OVA monomer units). Measurements were carried out at room temperature (around 20 °C).

3.1.2. Turbidity measurements

The turbidity (measured as ABS at 400 nm) of LA dispersions with and without OVAn (0.5 g/L) are show in Fig. 1C. System turbidity without OVAn increased linearly with the increase in LA concentration, suggesting the formation of LA supramolecular self-assemblies above the critical micelar concentration (CMC) (Sponton et al., 2015a). Nevertheless, in the presence of OVAn, system turbidity remained low and constant up to certain LA concentration from which started to increase. This behavior could be explained considering that LA binds to OVAn, and at OVAn saturation condition, unbound LA molecules start to associate with each other forming supramolecular self-assemblies. The two parts of the curve (constant turbidity and increasing turbidity) were fitted to linear regression model. Then, the intersection point was analytically calculated. The value corresponding to this point could be considered as a critical micelar concentration of LA in presence of OVAn (CMC'). The value of CMC' was 712 μM, 12 fold higher than pure LA CMC (60 μM) (Serth, Lautwein, Frech, Wittinghofer, & Pingoud, 1991). The LA concentration which saturate OVAn could be estimated as the difference between CMC' and CMC values (under assumption that CMC of pure LA would not change in presence of OVAn), resulting in 652 μM LA.

Because of OVAn are composed by aggregated OVA monomer units, a binding stoichiometry taking into account the OVA monomer molecular mass could be proposed (Le Maux et al., 2013). In these turbidity measurements, OVAn concentration was 0.5 g/L, which corresponds to 11.63 μM (in terms of OVA monomeric units). Hence, the binding stoichiometry LA:OVA was 652:11.63 = 56:1, i.e. 56 LA molecules would bind per OVA monomeric unit. This binding stoichiometry was in the same order to the one obtained by Le Maux et al. (2013) for linoleate-BLG nanoparticle complexes. Besides, a stoichiometry LA:OVA = 56:1 would be comparable to the one obtained by the modified Scatchard model using ANS fluorescence data (Eq. (1)).

3.2. Kinetic of LA-OVAn complex formation

Kinetic studies at different temperatures and LA/OVA ratios (L/P) were carried out. In this paper, a batch adsorption process was assumed, where OVAn was taken as adsorbent and LA as adsorbate. Kinetic assays were performed taking into account that LA forms supramolecular self-assemblies (conferring turbidity to the solution), which are disrupted in presence of OVAn producing a decrease in turbidity over time, due to LA-OVAn complexes formation (Sponton et al., 2015a).

Fig. 2 shows the relative turbidity (ABS at 400 nm) of LA dispersions (1 mM) as a function of time for different ligand/protein molar ratio (L/P = 21.5, 43.0, 86.0 and 172 LA mol/OVA monomer mol), at 20 °C, 30 °C and 40 °C. At the beginning time, a very fast decay of turbidity can be noted, suggesting a rapid adsorption process. This behavior could be explained by driving force increments provided by LA concentration gradient in the aqueous dispersions and by the existence of great number of available binding sites on OVAn (Liu & Zhang, 2015). It also can be noted that, at L/P = 21.5 and 43.0, at all temperatures, constant turbidity values were achieved, indicating that adsorption reached an equilibrium state (Fig. 2A and B). However, at L/P = 86.0 and 172 the adsorption equilibrium state during the testing time seemed to be reach only at 20 °C and 30 °C but not at 40 °C (Fig. 2C and D).

Fig. 2 also displays that, for a given temperature, the increase in L/P produced higher turbidity values, indicating an LA excess. Moreover, all measurements performed at 40 °C produced lower turbidity values than at 20 °C and 30 °C, suggesting that LA-OVAn complexes formation would be more favored at 40 °C, for a given L/P.

On the other hand, data shown in Fig. 2 were fitted to the proposed kinetic models (Eqs. (4) and (5)) in search of the best-fit to the data. The fitting to pseudo-first-order kinetic model was not good ($R^2 < 0.8$) (not shown); hence, it would not be suitable for describing the adsorption kinetic for LA-OVAn systems. However, the pseudo-second-order kinetic model shows the best fit with the experimental data ($R^2 > 0.997$). Hence, kinetic parameters were obtained at different L/P and temperatures through the last model (Table 1).

As it was mentioned, the parameter q_e is defined as adsorbed amount of LA by OVAn mass unit at the equilibrium (Yao & Chen,

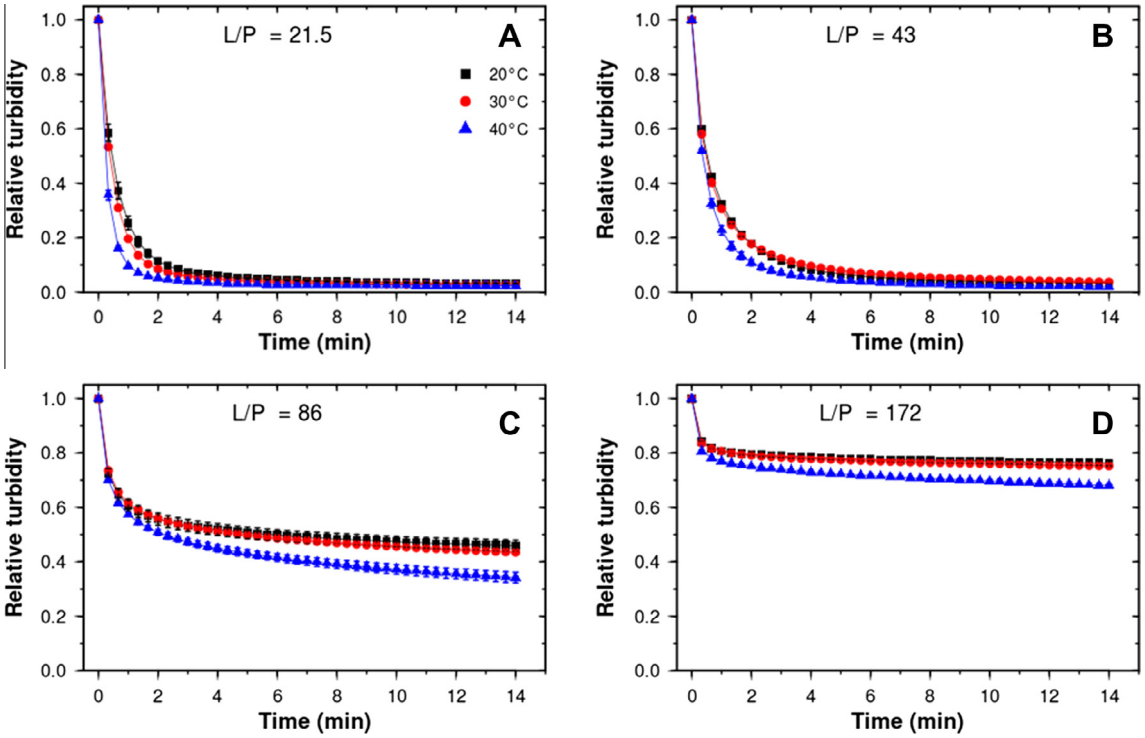

Fig. 2. Relative turbidity (ABS at 400 nm) of 1 mM LA dispersions in presence of OVAn as a function of time and temperature for different LA/OVAn molar ratio (L/P): A: 21.5; B: 43.0; C: 86.0; D: 172 LA mol/OVA mol.

Table 1
LA amount adsorbed by unit mass of adsorbent at equilibrium (q_e) (LA mol/OVA mol) and pseudo-second-order rate constants k_2 (OVA mol/LA mol*seg) for OVAn-LA complex formation at different temperatures and total LA amount to total OVAn amount ratios (L/P) (LA mol/OVA mol, on the basis of the OVA monomer units). Results are expressed as mean ± standard deviation. Different letters indicate significant differences ($p < 0.05$).

Temperature	L/P			
	21.5	43.0	86.0	172
q_e (LA mol/OVA monomer mol)				
20 °C	21.1 ± 0.0 a	42.8 ± 0.0 b	48.1 ± 1.6 c	41.6 ± 1.7 b
30 °C	21.2 ± 0.0 a	42.6 ± 0.0 b	50.8 ± 0.7 d	43.8 ± 1.1 b
40 °C	21.1 ± 0.0 a	42.8 ± 0.0 b	59.7 ± 1.9 f	57.3 ± 1.3 e
*k_2 (OVA monomer mol/LA mol*seg)*				
20 °C	$3.98 \pm 0.56 \times 10^{-3}$ a	$1.07 \pm 0.06 \times 10^{-3}$ a	$5.58 \pm 0.19 \times 10^{-4}$ c	$8.79 \pm 0.92 \times 10^{-4}$ c
30 °C	$5.32 \pm 0.16 \times 10^{-3}$ a	$1.01 \pm 0.76 \times 10^{-3}$ a	$4.04 \pm 0.16 \times 10^{-4}$ b	$6.64 \pm 0.00 \times 10^{-4}$ b
40 °C	$1.32 \pm 0.16 \times 10^{-2}$ b	$1.77 \pm 0.23 \times 10^{-3}$ b	$2.78 \pm 0.20 \times 10^{-4}$ a	$3.28 \pm 0.20 \times 10^{-4}$ a

2015). Hence, q_e could be considered as the mol number of adsorbed LA per OVA monomer mol. It can be seen that q_e values for L/P: 21.5 and 43.0, were similar to the corresponding L/P ratios (Table 1). This would mean that almost all LA molecules were bound to OVAn. Furthermore, q_e did not change significantly with the increase in temperature ($p > 0.05$), suggesting no effect on LA adsorption in terms of quantity. This behavior could be explained considering an excess of OVAn respect to LA. If LA binds to OVAn by mean of hydrophobic interactions (Sponton et al., 2015a), OVAn would have more affinity for LA at higher temperatures. Nevertheless, at L/P: 21.5 and 43, LA amount in the bulk would not be enough for additional adsorption promoted by the increase in temperature. On the other hand, for L/P: 86.0 and 172, the increase in temperature produced an increase in q_e values (Table 1). In these last conditions, LA is in excess respect to OVAn, conducting to additional adsorption promoted by temperature increase.

On the other hand, the maximum q_e value obtained at 20 °C ($q_e = 48.1 \pm 1.6$) (Table 1) was consistent with n value obtained from extrinsic fluorescence data fitted to the modified Scatchard model ($n = 49 \pm 2$) (Section 3.1). These results indicate that both techniques would be complementary and suitable for obtaining binding (or adsorption) stoichiometry. Moreover, this finding could confirm the assumption that in the extrinsic fluorescence approach, ANS did not displace LA from the complexes

The pseudo-second-order rate constants (k_2) for LA-OVAn complexes formation at different temperatures and L/P levels are also reported in Table 1. For L/P: 21.5 and 43.0, k_2 values at 40 °C was higher than the ones at 20 °C and 30 °C. Conversely, a decrease in k_2 value with the increase in temperature was registered for L/P: 86.0 and 172.

In order to interpret the behaviors described above, Arrhenius model was applied to obtain the activation energy involved in the adsorption process. The Arrhenius model is given by the following equation (Muench, Kruuv, & Lepock, 1996):

$$\ln k_{app} = \ln A_{app} - E_{app}/RT \quad (7)$$

where k_{app} is the apparent rate constant (in this case $k_{app} = k_2$ obtained from the pseudo-second-order model); A_{app} is the apparent pre-exponential factor; E_{app} is the apparent activation energy

involved in the adsorption process; R is the gas universal constant and T is the absolute temperature.

The activation energy can be obtained from the slope of $\ln k_{app}$ *versus* 1/T plot Eq. (7) by means of linear regression model. Fig. 3 shows $\ln k_{app}$ *versus* 1/T plot for LA-OVAn systems at different L/P. A good fitting ($R^2 > 0.8$) was obtained, with exception of L/P: 43.0 ($R^2 < 0.8$); however it was also included as an intermediate (transition) system. The E_{app} values (kJ/mol) obtained were: 44.1 (at 21.5 L/P); 18.5 (at 43.0 L/P); −26.4 (at 86.0 L/P) and −37.3 (at 172 L/P), i.e., a decrease in E_{app} values with L/P increment was observed. Positive E_{app} values were obtained for OVAn excess conditions (L/P: 21.5 and 43.0), while negative values were registered for LA excess conditions (L/P: 86.0 and 172). According to Sharma and Das (2012), activation energy values lower than 42 kJ/mol would indicate a physical adsorption phenomenon. The maximum activation energy value obtained for LA-OVAn system was 44.1 kJ/mol, which is very close to 42 kJ/mol, suggesting a physical absorption process. In agreement with a previous work, this physical adsorption process would be mediated by hydrophobic interactions (Sponton et al., 2015a).

In order to explain negative E_{app} values, the following adsorption mechanism can be supposed:

$$L_{free} \xrightarrow{k_{app}} L_{bound} \tag{8}$$

where L_{free} is the free LA (i.e., unbound LA); L_{bound} is LA bound to OVAn and k_{app} is the apparent rate constant (i.e., the pseudo-second-order rate constant, k_2). According to Muench et al., 1996, negative E_{app} values obtained from Arrhenius model could be explained by a molecular process which take place in two steps (i.e., three states). In this sense, L_{free} could be composed by two equilibrium species: LA self-assemblies (L_{SA}) and LA monomer (L_{sol}), i.e., $L_{free} = L_{SA} + L_{sol}$. Hence, Eq. (8) can be rewritten as follow:

$$L_{SA} \underset{k_{-1}}{\overset{k_1}{\leftrightarrows}} L_{sol} \xrightarrow{k'_2} L_{bound} \tag{9}$$

where k_1, k_{-1} and k'_2 are the rate constants. According to Muench et al. (1996) this model can be proposed if $k'_2 \ll k_1$ and k_{-1}.

For the first step in Eq. (9) the equilibrium constant, K_{eq}, can be defined, which can also be related with k'_2 and k_{app} as follow (Muench et al., 1996):

$$K_{eq} = \frac{k_{-1}}{k_1} = \frac{k'_2}{k_{app}} \Rightarrow k_{app} = \frac{k'_2}{K_{eq}} \tag{10}$$

Then, Eq. (10) could be re-defined considering Arrhenius equation for each constant (k_{app}, k'_2 and K_{eq}):

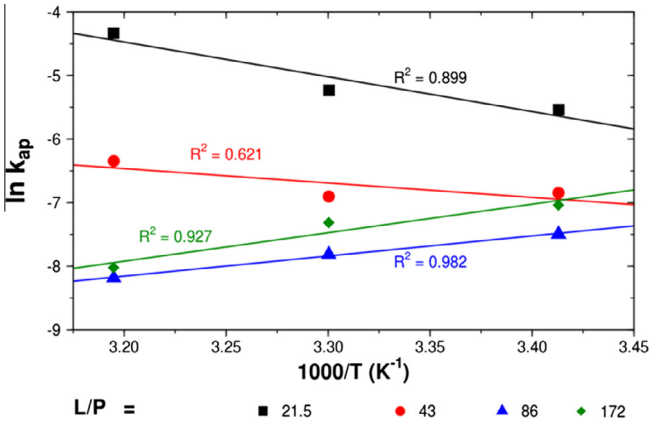

Fig. 3. Arrhenius plot for LA-OVAn adsorption at different total LA mol to total OVAn mol ratio (L/P).

$$e^{A_{app} - E_{app}/RT} = \frac{e^{A'_2 - E'_2/RT}}{e^{\Delta S - \Delta H/RT}} = e^{A'_2 - \Delta S - (E'_2 - \Delta H)/RT} \tag{11}$$

being A'_2 and E'_2 the pre-exponential factor and the activation energy, respectively, for the second step of Eq. (9); ΔS is the entropy change and ΔH is the enthalpy change which is defined as $\Delta H = E_{-1} - E_1$ (activation energies corresponding to the first step of Eq. (9)). Therefore, from Eq. (11), $E_{app} = E'_2 - \Delta H$.

In this way, a negative value of E_{app} (corresponding to the decreasing k'_2 values with temperature increase) would mean that $E'_2 - E_{-1} + E_1 < 0$, i.e., $E_{-1} > E'_2 + E_1$. Hence, the pathway $L_{sol} \rightarrow L_{SA}$ would be more temperature sensitive than the combined pathways, $L_{SA} \rightarrow L_{sol}$ and $L_{sol} \rightarrow L_{bound}$. In this sense, under conditions of LA excess, an increase in temperature would favor LA self-assemblies formation instead of both the disruption of LA self-assemblies and LA-OVAn complex formation (Muench et al., 1996).

This behavior seems to be L/P ratio dependent because at 172 L/P, the molecules number of LA bound per OVA monomer was lower than the one for 86.0 L/P, suggesting that at the highest L/P, $L_{sol} \rightarrow L_{bound}$ pathway would be less favored, i.e., less adsorption of LA monomers from the bulk solution.

In conclusion, LA-OVAn complexes formation could be characterized by a two-step mechanism: i) the disruption of LA self assemblies which would take place due to migration of LA molecules from the LA assemblies to the bulk and ii) the adsorption of LA monomers to OVAn. This mechanism was dependent on the L/P ratio and temperature.

3.3. Thermodynamics of LA-OVAn complexes formation

Adsorption thermodynamic studies involve the knowledge of parameters such as standard free energy (ΔG^0), enthalpy (ΔH^0) and entropy (ΔS^0) changes. These parameters allow describing partially the nature of the interaction between LA and OVAn (Joye et al., 2015). In order to obtain the adsorption thermodynamic parameters, the following equations can be used (Khan & Singh, 1987; Liu & Zhang, 2015):

$$\Delta G^0 = -RT \cdot \ln K_0 \tag{12}$$

$$\ln K_0 = \frac{\Delta S^0}{R} - \frac{\Delta H^0}{RT} \tag{13}$$

$$\Delta G^0 = -T \cdot \Delta S^0 + \Delta H^0 \tag{14}$$

where K_0 is the equilibrium constant. The K_0 value can be calculated from $\ln(C_e/q_e)$ *versus* C_e linear regression, being C_e the LA equilibrium concentration, obtained from Fig. 2at infinite time. This regression was made for each temperature (20 °C, 30 °C and 40 °C), including the $\ln(C_e/q_e)$ and C_e values corresponding to all L/P ratios. In the $\ln(C_e/q_e)$ *versus* C_e linear regression, the intercept corresponds to $\ln K_0$ (Khan & Singh, 1987). Hence, temperature dependence of K_0 gives information about the sign and magnitude of the system thermodynamic parameters (Joye et al., 2015). As can be noted in Eq. (13), ΔH^0 and ΔS^0 can be obtained from the slope and the intercept, respectively. The values of these parameters and K_0 are reported in Table 2. It is important to remark that

Table 2
Thermodynamic parameters for OVAn-LA adsorption process. ΔH^0 and ΔS^0 are not temperature dependent.

Temperature	K_0 (M^{-1})	ΔG^0 (kJ/mol)	ΔH^0 (kJ/mol)	ΔS^0 (J/mol K)	R^2
20 °C	8.72×10^5	−33.32	12.36	155.7	0.949
30 °C	9.67×10^5	−34.72			
40 °C	1.21×10^6	−36.44			

K_0 value at 20 °C was similar to the K_a value obtained from extrinsic fluorescence data fitted to the modified Scatchard model (Section 3.1). These results indicate that both techniques would be suitable and complementary for obtaining the binding (or adsorption) constant.

On the other hand, higher values of K_0 were observed with the increase in temperature. This behavior would explain the positive values of ΔH^0 and ΔS^0, indicating that LA adsorbs to OVAn by means of hydrophobic interactions (Chen et al., 2011). This finding would confirm previous results (Sponton et al., 2015a). Moreover, positive ΔH^0 value means that LA adsorption to OVAn would be an endothermic process (Joye et al., 2015; Liu & Zhang, 2015; Sharma & Das, 2012). While, negative ΔG^0 values and lower than −10 kJ/mol for all temperatures, suggest the spontaneous nature of the adsorption process through a physical mechanism. Besides, this observation is consistent with the finding obtained in the previous section (Liu & Zhang, 2015). Finally, the $-T{\cdot}\Delta S^0$ term in Eq. (14) was larger in magnitude than ΔH^0 term, so that the adsorption process would be entropically-driven (Santos, Manzanares, Murtomäki, & Kontturi, 2007), i.e. the solvent molecules surrounding both LA and OVAn arranged themselves in a less orderly way when the adsorption take place via hydrophobic interactions (Joye et al., 2015).

3.4. AFM imaging

Some morphological aspects of the OVAn and LA-OVAn complexes (L/P: 43) were determined using atomic force microscopy. AFM topography images (Fig. 4A and B) show particles with a high diameter/height ratio. According to Arzeni, Pérez, and Pilosof (2015), this observation could be explained taking into account that during the sample drying step involved in AFM technique, the particles crush on the mica surface. Besides, Fig. 4A and B show that LA-OVAn particle heights are greater than the OVAn ones, according to the lateral scale. These results could be due to the presence of LA into the OVAn structure and are in agreement with the idea of the proposed inside-out saturation mechanism, in which inner LA binding sites would be firstly filled (Section 3.1.1).

Fig. 4C and D display particles with a roughly rounded form and diameters lower than 100 nm, taking into account the micrograph scale. Moreover, several populations of particles, which include particles with diameters lower than 10 nm, can be observed. This population would correspond to non-aggregated OVA (native conformation). According to Weijers, Barneveld, Stuart, and Visschers (2003), part of the non aggregated OVA during heat treatment would corresponds to a stable intermediate fraction, i.e., monomers which are denatured but not aggregated. The non-aggregated OVA were not detected by DLS measurement, according to results presented in a previous work (Sponton et al., 2015a). This could be explained taking into account that in DLS technique, small particles may be underestimated due to large particles scatter light with a greater intensity than the small ones (Arzeni et al., 2015). About this, Arzeni et al. (2015) determined size of non-filtered and filtered samples of protein nanoparticles and they found that the smallest size populations which were not detected in the non-filtered sample were effectively detected in the filtered ones. Hence, AFM would give more detailed information about the identification of size populations than DLS technique. However, information obtained through both techniques would be complementary giving a deepest characterization for this kind of nanoparticles.

4. Conclusion

Stoichiometric, kinetic and thermodynamic parameters of LA-OVAn complexes formation could be obtained from extrinsic fluorescence and turbidity measurements at different temperatures and L/P ratios. It was demonstrated that binding analysis can be performed monitoring the extrinsic fluorescence behavior of LA-OVAn systems, in order to obtain binding parameters (n and K_a) in close relationship to the ones obtained by the turbidity approach. On the other hand, LA-OVAn complexes formation was

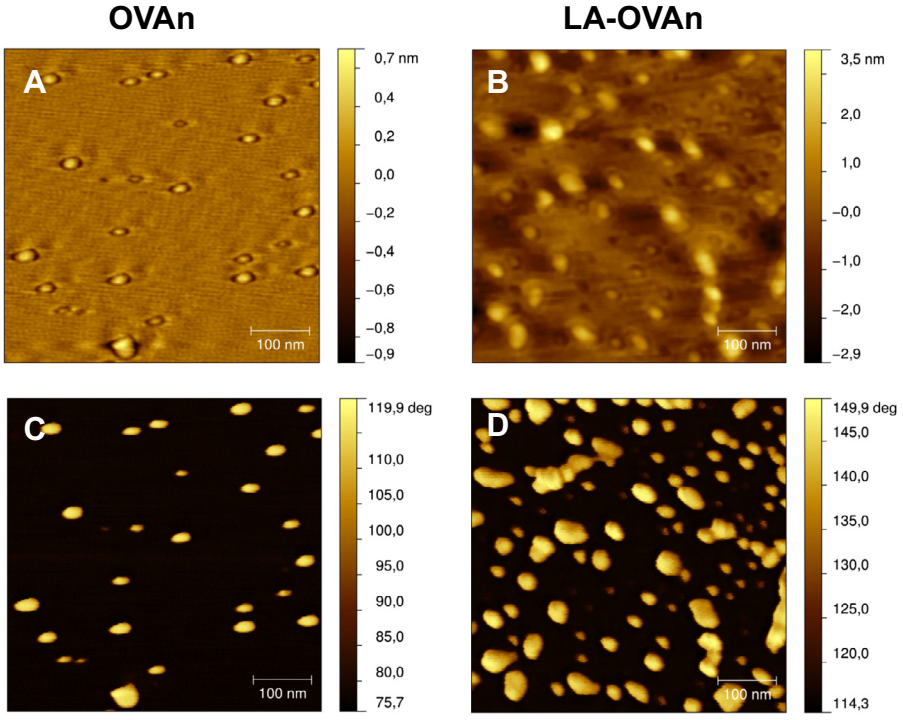

Fig. 4. Topographical (A and B) and phase (C and D) AFM images of OVAn and LA-OVAn complexes.

studied considering an adsorption process, which is not often proposed for this kind of systems. Thermodynamic parameters were obtained which allowed a wider characterization. Finally, AFM imaging revealed some structural aspects of LA-OVAn complex formation. The information obtained in this work resulted of basic and technological interest for defining the more appropriate conditions to develop innovative nutraceutical vehiculization systems.

Acknowledgements

Authors acknowledge the financial support of the following projects: CAI+D-2013-50120110100-171-LI (UNL) and PICT-2014-2636 (ANPCyT), and especially to CONICET – Argentina for the PhD fellowships awarded to Osvaldo E. Sponton. Moreover, authors thank to José L. Fernández for AFM imaging acquisition.

References

Albani, J. R. (2004). *Structure and dynamics of macromolecules: Absorption and fluorescence studies*.Paris: Elsevier.

Arzeni, C., Pérez, O. E., & Pilosof, A. M. R. (2015). Power ultrasound assisted design of egg albumin nanoparticles. *Food Biophysics, 10*(4), 439–446.

Chen, T., Zhu, S., Cao, H., Shang, Y., Wang, M., Jiang, G., ... Lu, T. (2011). Studies on the interaction of salvianolic acid B with human hemoglobin by multi-spectroscopic techniques. *Spectrochimica Acta Part A, 78*, 1295–1301.

Croguennec, T., Renault, A., Beaufils, S., Dubois, J., & Pezennec, S. (2007). Interfacial properties of heat-treated ovalbumin. *Journal of Colloid and Interface Science, 315*, 627–636.

Fioramonti, S. A., Arzeni, C., Pilosof, A. M. R., Rubiolo, A. C., & Santiago, L. G. (2015). Influence of freezing temperature and maltodextrin concentration on stability of linseed oil-in-water multilayer emulsions. *Journal of Food Engineering, 156*, 31–38.

Fontana, A., Spolaore, B., & Polverino de Laureto, P. (2013). The biological activities of protein/oleic acid complexes reside in the fatty acid. *Biochimica et Biophysica Acta, 1834*, 1125–1143.

Gutiérrez, F. J., Albillos, S. M., Casas-Sanz, E., Cruz, Z., García-Estrada, C., García-Guerra, A., et al. (2013). Methods for the nanoencapsulation of β-carotene in the food sector. *Trends in Food Science and Technology, 32*, 73–83.

Joye, I. J., Davidov-Pardo, G., Ludescher, R. D., & McClements, D. J. (2015). Fluorescence quenching study of resveratrol binding to zein and gliadin: Towards a more rational approach to resveratrol encapsulation using water-insoluble proteins. *Food Chemistry, 185*, 261–267.

Khan, A. A., & Singh, R. P. (1987). Adsorption thermodynamics of carbofuran on Sn (IV) arsenosilicate in H^+, Na^+ and Ca^{2+} forms. *Colloids and Surfaces, 24*, 33–42.

Lange, D. C., Kothari, R., Patel, R. C., & Patel, S. C. (1998). Retinol and retinoic acid bind to a surface cleft in bovine β-lactoglobulin: A method of binding site determination using fluorescence resonance energy transfer. *Biophysical Chemistry, 74*, 45–51.

Le Maux, S., Bouhallab, S., Giblin, L., Brodkorb, A., & Croguennec, T. (2013). Complexes between linoleate and native or aggregated β-lactoglobulin: Interaction parameters and in vitro cytotoxic effect. *Food Chemistry, 141*, 2305–2313.

Liu, X., & Zhang, L. (2015). Removal of phosphate anions using the modified chitosan beads: Adsorption kinetic, isotherm and mechanism studies. *Powder Technology, 277*, 112–119.

McClements, D. J., & Li, Y. (2010). Structured emulsion-based delivery systems: Controlling the digestion and release of lipophilic food components. *Advances in Colloid Interface Science, 159*, 213–228.

Muench, J. L., Kruuv, J., & Lepock, J. R. (1996). A two-step reversible-irreversible model can account for a negative activation energy in an Arrhenius plot. *Cryobiology, 33*, 253–259.

Moyon, N. S., Islam, M. M., Phukan, S., & Mitra, S. (2013). Fluorescence modulation and associative behavior of lumazine in hydrophobic domain of micelles and bovine serum albumin. *Journal of Photochemistry and Photobiology B: Biology, 121*, 37–45.

Muresan, S., van der Bent, A., & de Wolf, F. A. (2001). Interaction of β-lactoglobulin with small hydrophobic ligands as monitored by fluorometry and equilibrium dialysis: Nonlinear quenching effects related to protein-protein association. *Journal of Agricultural and Food Chemistry, 49*, 2609–2618.

Perez, A. A., Carrera Sánchez, C., Rodríguez Patino, J., Rubiolo, A., & Santiago, L. G. (2012). Effect of enzymatic hydrolysis and polysaccharide addition on the β-lactoglobulin adsorption at the air–water interface. *Journal of Food Engineering, 109*(4), 712–720.

Perez, A. A., Andermatten, R. B., Rubiolo, A. C., & Santiago, L. G. (2014). β-Lactoglobulin heat-induced aggregates as carriers of polyunsaturated fatty acids. *Food Chemistry, 158*, 66–72.

Perez, A. A., Sponton, O. E., Andermatten, R. B., Rubiolo, A. C., & Santiago, L. G. (2015). Biopolymer nanoparticles designed for polyunsaturated fatty acid vehiculization: Protein–polysaccharide ratio study. *Food Chemistry, 188*, 543–550.

Rhodes, A. A., Swartz, B. L., Hosler, E. R., Snyder, D. L., Benitez, K. M., Chohan, B. S., & Basu, S. (2014). Static quenching of tryptophan fluorescence in proteins by a dioxomolybdenum(VI) thiolate complex. *Journal of Photochemistry and Photobiology A: Chemistry, 293*, 81–87.

Ruxton, C. H. S., Reed, S. C., Simpson, M. J. A., & Millington, K. J. (2004). The health benefits of omega-3 polyunsaturated fatty acids: A review of the evidence. *Journal of Human Nutrition and Dietetics, 17*, 449–459.

Santos, H. A., Manzanares, J. A., Murtomäki, L., & Kontturi, K. (2007). Thermodynamic analysis of binding between drugs and glycosaminoglycans by isothermal titration calorimetry and fluorescence spectroscopy. *European Journal of Pharmaceutical Sciences, 3*(2), 105–114.

Serth, J., Lautwein, A., Frech, M., Wittinghofer, A., & Pingoud, A. (1991). The inhibition of the GTPase activating protein Ha-ras interaction by acidic lipids is due to physical association of the C-terminal domain of the GTPase activating protein with micellar structures. *The EMBO Journal, 10*(6), 1325–1330.

Sharma, P., & Das, M. R. (2012). Removal of a cationic dye from aqueous solution using graphene oxide nanosheets: Investigation of adsorption parameters. *Journal of Chemical & Engineering Data, 58*(1), 151–158.

Sponton, O. E., Perez, A. A., Carrara, C., & Santiago, L. G. (2014). Effect of limited enzymatic hydrolysis on linoleic acid binding properties of β-lactoglobulin. *Food Chemistry, 146*, 577–582.

Sponton, O. E., Perez, A. A., Carrara, C. R., & Santiago, L. G. (2015a). Linoleic acid binding properties of ovalbumin nanoparticles. *Colloids and Surfaces B: Biointerfaces, 128*, 219–226.

Sponton, O. E., Perez, A. A., Carrara, C. R., & Santiago, L. G. (2015b). Impact of environment conditions on physicochemical characteristics of ovalbumin heat induced nanoparticles and on their ability to bind PUFAs. *Food Hydrocolloids, 48*, 165–173.

Takikawa, H., & Kaplowitz, N. (1986). Binding of bile acids, oleic acid, and organic anions by rat and human hepatic Z protein. *Archives of Biochemistry and Biophysics, 251*(1), 385–392.

Wang, R., Yin, Y., Li, H., Wang, Y., Pu, J., Wang, R., ... Wang, R. (2013). Comparative study of the interactions between ovalbumin and three alkaloids by spectrofluorimetry. *Molecular Biology Reports, 40*, 3409–3418.

Weijers, M., Barneveld, P. A., Stuart, M. A. C., & Visschers, R. W. (2003). Heat-induced denaturation and aggregation of ovalbumin a neutral pH described by irreversible first-order kinetics. *Protein Science, 12*, 2693–2703.

Yao, C., & Chen, T. (2015). A new simplified method for estimating film mass transfer and surface diffusion coefficients from batch adsorption kinetic data. *Chemical Engineering Journal, 265*, 93–99.

Zimet, P., & Livney, Y. D. (2009). Beta-lactoglobulin and its nanocomplexes with pectin as vehicles for ω-3 polyunsaturated fatty acids. *Food Hydrocolloids, 23*(4), 1120–1126.